Check for updates

Morpho-molecular diversity and phylogeny of *Bysmatrum* (Dinophyceae) from the South China Sea and France

Zhaohe Luo[a], Zhen Fei Lim[b], Kenneth Neil Mertens[c], Pieter Gurdebeke[d], Kara Bogus[e], M. Consuelo Carbonell-Moore[f], Henk Vrielinck[g], Chui Pin Leaw[b], Po Teen Lim[b], Nicolas Chomérat[c], Xintian Li[a] and Haifeng Gu[a]

[a]Third Institute of Oceanography, SOA, Xiamen 361005, China; [b]Institute of Ocean and Earth Sciences, University of Malaya, 16310 Bachok, Kelantan, Malaysia; [c]Ifremer, LER BO, Station de Biologie Marine, Place de la Croix, BP40537, F-29185 Concarneau CEDEX, France; [d]Research Unit Palaeontology, Department of Geology, Ghent University, Krijgslaan 281, S8, B-9000 Gent, Belgium; [e]International Ocean Discovery Program, Texas A&M University, College Station, TX, 77845, USA; [f]Oregon State University, Department of Botany and Plant Pathology, College of Agricultural Sciences, 2082 Cordley Hall, Corvallis, OR 97331-2902, USA; [g]Department of Solid State Sciences, Ghent University, Krijgslaan 281, S1, B-9000 Gent, Belgium

ABSTRACT
The dinoflagellate genus *Bysmatrum* encompasses five epibenthic or tide-pool species and has been characterized by separated anterior intercalary plates. In the present study, we obtained six strains of *Bysmatrum* from the South China Sea and French Atlantic coast by isolating single cells/cysts from plankton and sediment samples. All strains were examined with light microscopy and scanning electron microscopy. Based on morphological observations, three strains were identified as *Bysmatrum subsalsum*, characterized by the elongated and rectangular first and a hexagonal second anterior intercalary plate. They differ from each other in the number of sulcal lists and the configuration of the first anterior intercalary plate. One strain was identified as *Bysmatrum gregarium* and the other two as *Bysmatrum granulosum*. The cyst-theca relationship of *B. subsalsum* from the French Atlantic was established by incubation of the cyst, and the geochemical composition of the cyst wall was measured through micro-Fourier transform infrared spectroscopy. *Bysmatrum subsalsum* from Malaysia shows a bright red stigma in the sulcal area under light microscopy, which was confirmed with transmission electron microscopy: it was identified as a type B eyespot. Small subunit ribosomal DNA (SSU rDNA), partial large subunit ribosomal DNA (LSU rDNA) and internal transcribed spacer (ITS) sequences were obtained from all six strains. The maximum likelihood and Bayesian inference analysis based on concatenated SSU, ITS and LSU sequences revealed that *Bysmatrum* is monophyletic and nested within Peridiniales. Our strains of *B. subsalsum* form a new ribotype in the molecular phylogeny (designated as ribotype B). The genetic distance based on ITS sequences among *Bysmatrum* species ranged from 0.34 to 0.47 and those genetic distances at the intraspecific level of *B. subsalsum* could reach 0.41, supporting the possibility of hidden crypticity within *B. subsalsum*.

Introduction

The dinoflagellate genus *Bysmatrum* Faust & Steidinger was erected in 1998 (Faust & Steidinger, 1998). The plate formula of *Bysmatrum* is Po, X, 4′, 3a, 7″, 6C, 4S, 5‴, 2⁗ with *Bysmatrum subsalsum* as type species. The type was initially assigned to *Peridinium* by Ostenfeld (1908) and transferred later to *Scrippsiella* Balech ex Loeblich by Steidinger & Balech (1977). However, *Bysmatrum* differs from *Scrippsiella* mainly in that the anterior intercalary plates 2a and 3a are separated by the third apical plate (Faust & Steidinger, 1998). Since then, two other *Scrippsiella* species were transferred to *Bysmatrum*: *Bysmatrum arenicola* Horiguchi & Pienaar (although *Scrippsiella arenicola* was invalidly published by Horiguchi & Pienaar, 1988a), and *B. gregarium* (Lombard & Capon) Horiguchi & Hoppenrath (= *B. caponii*, illegitimate). Three other

species have been assigned to *Bysmatrum*: *B. granulosum* Ten-Hage, Quod, Turquet & Couté, *B. teres* Murray, Hoppenrath, Larsen & Patterson and *B. australis* Dawut, Sym, Suda & Horiguchi (Ten-Hage *et al.*, 2001; Murray *et al.*, 2006; Dawut *et al.*, 2018). *Peridinium sociale* (Henneguy) Biecheler also possesses three intercalary plates with 2a and 3a separated (Biecheler, 1952), and thus might belong to *Bysmatrum* as well (Murray *et al.*, 2006). In fact, Biecheler (1952, p. 59) regarded *Peridinium sociale* as a junior synonym of *P. subsalsum*. Useful characteristics to differentiate *Bysmatrum* species at the interspecific level include overall cell shape, plate ornamentation, cingulum displacement, the position of the nucleus and the shape of the apical pore complex (Horiguchi, 1983; Murray *et al.*, 2006).

Bysmatrum species are considered photosynthetic, benthic dinoflagellates (Hoppenrath *et al.*, 2014), although some specimens of *B. subsalsum* have been

recovered from plankton, as well as floating detritus, sand and macroalgae (Faust, 1996). *Bysmatrum teres* was reported to be sand-dwelling (Murray *et al.*, 2006) and *B. granulosum* has been recovered from surface sediment, coral rubble and macroalgal turf (Ten-Hage *et al.*, 2001). *Bysmatrum arenicola, B. gregarium* and *B. austrafrum* are considered to inhabit tide pools (Horiguchi & Pienaar 1988*a*, 1988*b*; Dawut *et al.*, 2018). *Bysmatrum* species are found in tropical to temperate waters (Hoppenrath *et al.*, 2014) and may form blooms: *B. subsalsum* in mangrove detritus and salt marshes (Anglès *et al.*, 2017), *B. gregarium* in tidal pools (Lombard & Capon, 1971) and *B. arenicola* on sandy sediments (Horiguchi & Pienaar, 1988*b*).

The molecular characterization of *Bysmatrum* is in its infancy: four out of the six described species have been sequenced: *B. subsalsum, B. gregarium, B. arenicola* and *B. austrafrum* have ribosomal DNA (rDNA) sequences available (Gottschling *et al.*, 2012; Jeong *et al.*, 2012; Anglès *et al.*, 2017; Dawut *et al.*, 2018). For *B. subsalsum*, only sequences from the Mediterranean Sea are available and two distinct clades in their small subunit (SSU), internal transcribed spacer (ITS) and large subunit (LSU) rDNA based phylogenies suggest hidden cryptic species (Anglès *et al.*, 2017). Despite the peridinoid tabulation, the closest relative and higher rank of *Bysmatrum* remain unresolved (Gottschling *et al.*, 2012; Anglès *et al.*, 2017; Dawut *et al.*, 2018), and the phylogenetic relationships among *Bysmatrum* species have not been elucidated. *Bysmatrum subsalsum, B. gregarium, B. granulosum* and *B. austrafrum* were described as possessing an eyespot (Faust & Steidinger, 1998; Ten-Hage *et al.*, 2001; Jeong *et al.*, 2012; Dawut *et al.*, 2018), but detailed examination using transmission electron microscopy (TEM), which is necessary to characterize the eyespot, has only been carried out on *B. austrafrum*. The eyespot is considered of systematic importance at family level for other dinoflagellates (Lindberg *et al.*, 2005; Moestrup & Daugbjerg, 2007), and its description may help better understand the systematic position of *Bysmatrum* within the Peridiniales. Information on plate overlap is helpful to identify possible plate homology, and will contribute to the understanding of the systematic relationship of armoured dinoflagellates (Netzel & Dürr, 1984).

Among the 2000 extant dinoflagellate species, only around 15% have been related to resting cysts (Head, 1996), although many recent studies have described new cyst-motile stage relationships (e.g. Gu *et al.*, 2015*a*, *b*). When describing *Bysmatrum subsalsum* (as *Peridinium subsalsum* Ostenfeld), Ostenfeld (1908, p. 167) mentioned an ovoid cyst without illustration. Spherical to ovoid cysts were produced by *B. subsalsum* in culture (Gottschling *et al.*, 2012; Anglès *et al.*, 2017) while cysts with the typical plate pattern of *B.*

subsalsum were identified in recent sediments, and survived palynological treatment (Limoges *et al.*, 2015). In addition, unidentified *Bysmatrum* cells were germinated from ellipsoidal or ovoid cysts found in surface sediment from the Mediterranean lagoons and bays (Satta *et al.*, 2013*a*, *b*). The cyst–theca relationship of *Bysmatrum* has only been established through germination experiments for Mediterranean *B. subsalsum* (Anglès *et al.*, 2017). Germination of more *Bysmatrum* cysts from elsewhere will be helpful to fully understand the diversity within the genus. The geochemical composition of the cyst wall can be studied with the aid of micro-Fourier transform infrared spectroscopy. Bogus *et al.* (2014) concluded that cyst walls of autotrophic and heterotrophic species differ in their chemical composition, thus are useful indicators for infering nutrient strategies.

To increase knowledge on the morpho-molecular diversity of *Bysmatrum* species and to explore their phylogenetic relationships, five strains belonging to three species were established from the South China Sea (*B. granulosum, B. gregarium, B. subsalsum*), and one strain from the French Atlantic coast (*B. subsalsum*). Additionally, the morphology of their thecate stages was examined and the molecular phylogeny was inferred with concatenated SSU, LSU rDNA and ITS sequences. Finally, the cyst morphology, cyst wall chemistry and ultrastructure (with a focus on the type of eyespot) were analysed for *B. subsalsum*.

Materials and methods

Sample collection and treatment

One litre surface water samples were collected from the South China Sea (China and Malaysia) using a plastic bottle and concentrated through a 20 µm filter, and the upper 5 cm of sand samples were collected from nearby Rawa Island (Malaysia) by divers. The sand samples were stirred vigorously to detach the epibenthic cells and the suspension settled in a composite settling chamber. The settled materials were rinsed with filtered seawater and transferred into a polycarbonate bottle. Single *Bysmatrum* cells were isolated by means of drawn-out Pasteur pipettes under an AE30 inverted microscope (Motic, Xiamen, China) and established into clonal cultures. Three strains of *Bysmatrum* were established by isolating a single cell from plankton samples, and two strains from the sand sample (Table 1). Sediment sampling was done using an Ekman grab on 15 and 19 April 2016 in a shallow natural reservoir used for oyster cleansing before commercialization (water depth 1.2–1.5 m). The small basin is located north of the community of Gujan-Mestras in the Gironde region of south-western France. The top 2 cm of sediment from France were sliced off and stored in

Table 1. *Bysmatrum* strains examined in the present study, including the collection locality, coordinates and collection date.

Species	Strains	Source	Collection locality	Coordinates	Collection date
B. subsalsum	TBBYS02	Plankton	Tok Bali, Malaysia	05°51'53.81" N, 102°30'21.16" E	23 Sep 2015
B. subsalsum	TBBYS03	Plankton	Tok Bali, Malaysia	05°51'53.81" N, 102°30'21.16" E	23 Sep 2015
B. subsalsum	TIO406	Sediment	Gironde, France	44°38'11"N, 1°04'00" W	15 & 19 April 2016
B. gregarium	TIO316	Plankton	Beihai, China	21°24'38.78" N, 109°10'13.47" E	3 Dec 2015
B. granulosum	SP004	Sediment	Perhentian Island, Malaysia	05°52'51.50" N, 102°44'34.88" E	17 May 2017
B. granulosum	A10-P14-R2	Sediment	Rawa Island, Malaysia	05°57'44.45" N, 102°40'53.26" E	7 Sep 2015

the dark at 4°C until further treatment. Approximately 5 g of wet sediment was mixed with 20 ml of filtered seawater and stirred vigorously to dislodge detrital particles. The settled material was subsequently sieved through 120 µm and 10 µm filters. Single cysts were isolated with a micropipette under an inverted Eclipse TS100 (Nikon, Tokyo, Japan) microscope and incubated in small containers with f/2-Si medium (Guillard & Ryther, 1962) at 20°C, 90 µm photons m^{-2}s^{-1} under a 12:12 h light: dark cycle. Another strain (TIO406) was established in clonal cultures under the same culture conditions (Table 1).

Morphological study of thecate stages and cysts

Live cells of all strains were examined and photographed using a Zeiss Axio Imager light microscope (Carl Zeiss, Göttingen, Germany) equipped with a Zeiss Axiocam HRc digital camera. Cell size of 13–40 cells was measured using Axiovision (4.8.2 version) software at 1000× magnification. Fluorescence brightener Calcofluor white (Sigma Adrich, St. Louis, USA) was used to stain the plates following the method of Fritz & Triemer (1985). To observe the shape and location of the nucleus, cells were stained with 1:100,000 Sybr Green (Sigma Aldrich, St. Louis, USA) for 1 min, and photographed under the Zeiss fluorescence microscope with a Zeiss-38 filter set (excitation BP 470/40, beam splitter FT 495, emission BP 525/50). Cysts of *B. subsalsum* from Gironde, France with cell contents were photographed and measured using an Olympus DP72 camera mounted on a BX41 microscope with 100× oil immersion objectives.

For scanning electron microscopy (SEM), mid-exponential batch cultures of all strains were concentrated by a Universal 320 R centrifuge (Hettich-Zentrifugen, Tuttlingen, Germany) at 850 *g* for 10 min at room temperature. The pellet was treated as described by Tillmann et al. (2009) to strip off the outer cell membrane. Cells were fixed with 2.5% glutaraldehyde for 3 h at 8°C, rinsed with Milli-Q water twice and post-fixed with 1% OsO$_4$ overnight at 8°C. The supernatant was removed and the settled cells were transferred to a coverslip coated with poly-L-lysine (molecular weight 70,000–150,000). The cells attached to the cover slip were rinsed in Milli-Q water twice. The samples were then dehydrated in a graded ethanol series (10%, 30%, 50%, 70%, 90% and 3× in 100%, 10 min at each step),

critical point dried (K850 Critical Point Dryer, Quorum/Emitech, West Sussex, UK), sputter-coated with gold, and examined with a Zeiss Sigma FE (Carl Zeiss Inc., Oberkochen, Germany) scanning electron microscope at Xiamen University, China.

Single cysts of *Bysmatrum subsalsum* from France were picked from the residue filtered using polycarbonate membrane filters (Millipore, Billerica, MA, USA, GTTP Isopore, 0.22 µm pore size), sputter coated with gold, and examined using a FEI Quanta 200 SEM with an electron acceleration of 2.5 to 5 kV at IFREMER (Plouzané, France).

The plate overlap was derived for *B. subsalsum* from SEM micrographs. For *Vulcanodinium rugosum*, SEM micrographs previously obtained by Nézan & Chomérat (2011) were used. For *Parvodinium umbonatum*, new SEM micrographs were made for thecae from a plankton sample from a lake to the north of Bergen, Norway (60.47°N, 4.95°E). Labelling of tabulation follows a modified Kofoid system that recognizes homologues (e.g. Fensome et al., 1993). The sulcal plate labelling is according to Balech (1980).

Transmission electron microscopy (TEM) of *B. subsalsum*

Mid-exponential batch cultures of strains TBBYS02 and TBBYS03 were fixed in 2.5% glutaraldehyde in phosphate buffered saline (PBS, 0.1 M at pH 7.4) for 1 h, concentrated by centrifugation and then washed three times with the same PBS for 10 min each. They were post-fixed in 1% OsO$_4$ overnight at 4°C and washed three times with the same PBS for 10 min each. The cells were then dehydrated through a graded ethanol series (10, 30, 50, 70, 95, 3× in 100%, 10 min at each step). The pellet was embedded in Spurr's resin (Spurr, 1969) and sectioned with a Reichert Ultracut E microtome (Leica, Vienna, Austria), mounted on Formvar-coated grids, stained with uranyl acetate and lead citrate, and observed in a JEOL JEM-100 transmission electron microscope (JEOL, Tokyo, Japan).

Micro-Fourier infrared spectroscopy

For micro-FTIR analyses, cysts without cell contents of *B. subsalsum* were isolated from palynological residues, and were rinsed three times with organic solvents (methanol and dichloromethane) and MilliQ water to remove polar and apolar compounds. Cysts

were placed on a gold-coated mirror, dried, and then analysed in reflective mode with 100 scans from 4000–600 cm^{-1} on a Hyperion 3000 FT-IR microscope (Bruker Optics, Elltingen, Allemagne) with a 15× objective, resulting in a consistent 50×50 μm window. The raw spectra (n=3) were subjected to background subtraction, atmospheric correction and rubberband baseline correction (5 iterations).

PCR amplifications and sequencing

The total algal DNA of six *Bysmatrum* strains (Table 1) was extracted from 10 ml of exponentially growing cultures using a MiniBEST Universal DNA Extraction Kit (Takara, Tokyo, Japan) according to the manufacturer's protocol. PCR amplifications were carried out using 1×PCR buffer, 50 μM dNTP mixture, 0.2 μM of each primer, 10 ng of template genomic DNA, and 1 U of ExTaq DNA Polymerase (Takara, Tokyo, Japan) in 50 μl reactions. The SSU rDNA was amplified using the primers PRIMERA/PRIMERB (Medlin *et al.*, 1988). The LSU rDNA was amplified using the primers D1R/ 28-1483R (Scholin *et al.*, 1994; Daugbjerg *et al.*, 2000). The total ITS1–5.8S–ITS2 was amplified using ITSA/ ITSB primers (Adachi *et al.*, 1996). The thermal cycle procedure was 4 min at 94°C, followed by 30 cycles of 1 min at 94°C, 1 min at 45°C, 1 min at 72°C, and final extension of 7 min at 72°C with a Mastercycler (Eppendorf, Hamburg, Germany). The PCR product was purified using a DNA purification kit (Shengong, Shanghai, China) and sequenced directly in both directions on an ABI PRISM 3730XL (Applied Biosystems, Foster City, California, USA) following the manufacturer's instructions.

Cells of *Vulcanodinium rugosum* were isolated using a micropipette with the Olympus IX70 inverted light microscope, and deposited on a glass slide. Then, the cell was rinsed into two drops of double distilled water (ddH$_2$O) before transfer to a 0.2 ml PCR tube containing 3 μl of ddH$_2$O. PCR tubes were stored at −20°C before the direct PCR amplifications. Each PCR tube was thawed before adding 25 pmol of each primer and 12.5 μl of PCR Master Mix 1X (Promega, Madison, Wisconsin, USA) containing the Taq DNA polymerase, dNTPs, MgCl$_2$ and reaction buffers. Three nuclear markers: SSU rDNA, LSU rDNA, internal transcribed spacer region (ITS1-5.8S rDNA-ITS2) were amplified using different cells with several pairs of primers (table 1 in Nézan *et al.*, 2012). The PCRs were performed in a Mastercycler Personal (Eppendorf, Hamburg, Germany) as follows: one initial denaturation step at 94°C for 2 min, followed by 45 cycles at 94°C for 30 s, 52°C for 30 s, and 72°C for 4 min, and a final elongation at 72°C for 5 min. The PCR products were purified using the Wizard SV Gel and PCR Clean-up system (Promega) according to the manufacturer's recommendations. Then, they were sequenced directly using the ABI PRISM BigDye Terminator Cycle Sequencing Kit (Applied Biosystems, Carlsbad, CA, USA).

Newly obtained sequences were deposited in GenBank with accession numbers MG826100 to MG826115 and MG826360 to MG826367 (Supplementary table S1).

Sequence alignment and phylogenetic analysis

Newly obtained *Bysmatrum* sequences (nuclear-encoded SSU, partial LSU rDNA and ITS) were incorporated into a systematically representative set of dinoflagellates available in GenBank. Sequences were aligned using MAFFT v7.110 (Katoh & Standley, 2013) online program (http://mafft.cbrc.jp/alignment/ server/) with default settings. Alignments were manually checked with BioEdit v. 7.0.5 (Hall 1999). For Bayesian inference (BI), the program jModelTest (Posada 2008) was used to select the most appropriate model of molecular evolution with Akaike Information Criterion (AIC). Bayesian reconstruction of the data matrix was performed using MrBayes 3.2 (Ronquist & Huelsenbeck, 2003) with the best-fitting substitution model (GTR+G). Four Markov chain Monte Carlo (MCMC) chains ran for 6 000 000 generations, sampling every 100 generations. The first 10% of burn-in trees were discarded. A majority rule consensus tree was created in order to examine the posterior probabilities of each clade. Maximum likelihood (ML) analyses were conducted with RaxML v7.2.6 (Stamatakis, 2006) on the T-REX web server (Boc *et al.*, 2012) using the model GTR+G. Node support was assessed with 1000 bootstrap replicates.

Multiple ITS1-5.8S-ITS2 sequences of *Bysmatrum* species were aligned using MAFFT v7.110 (Katoh & Standley, 2013) online program (http://mafft.cbrc.jp/ alignment/server/) with default settings. Completed alignments were saved as NEXUS files and imported into PAUP*4b10 software (Swofford, 2002) so that divergence rates could be estimated using simple uncorrected pairwise (p) distance matrices.

Results

Morphology

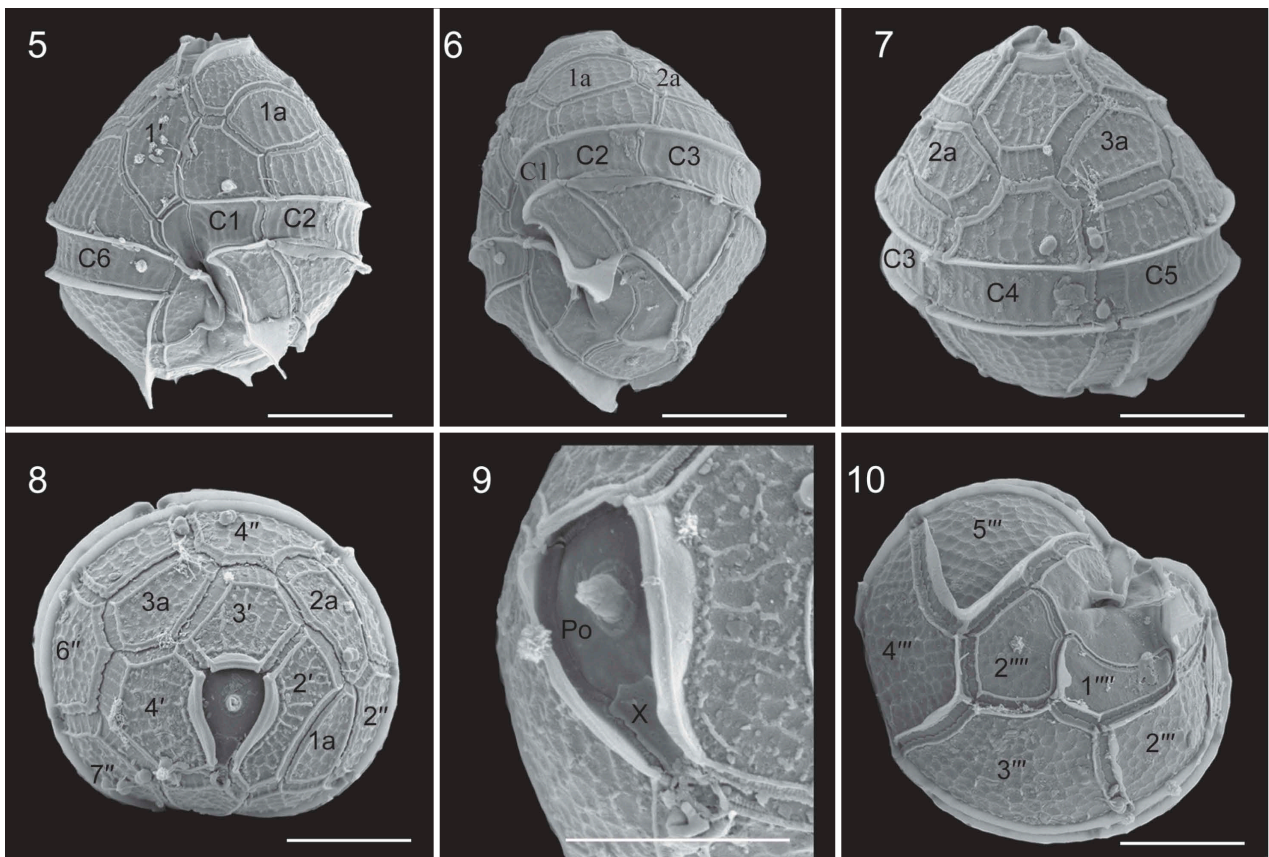*Bysmatrum subsalsum*: Cysts of *Bysmatrum subsalsum* from Gironde, France were 30.0–40.9 μm long (mean = 36.0±3.4 μm, n=14) and 26.0–34.3 μm wide (mean =31.6±2.8 μm, n=14). They had a conical epitheca, and a round hypotheca (Fig. 1). The cysts possessed numerous golden granules and a red accumulation body in the sulcal area (Figs 1, 2). Plates were clearly visible and were identical to the thecal plates (Figs 3, 4).

Cells of strain TIO406 from France were 22.7–31.7 μm long (mean =27.3±3.2 μm, n=15) and 22.0–29.4 μm wide (mean =23.9±2.3 μm, n=15). Under SEM, cysts and vegetative cells of *Bysmatrum subsalsum* from France
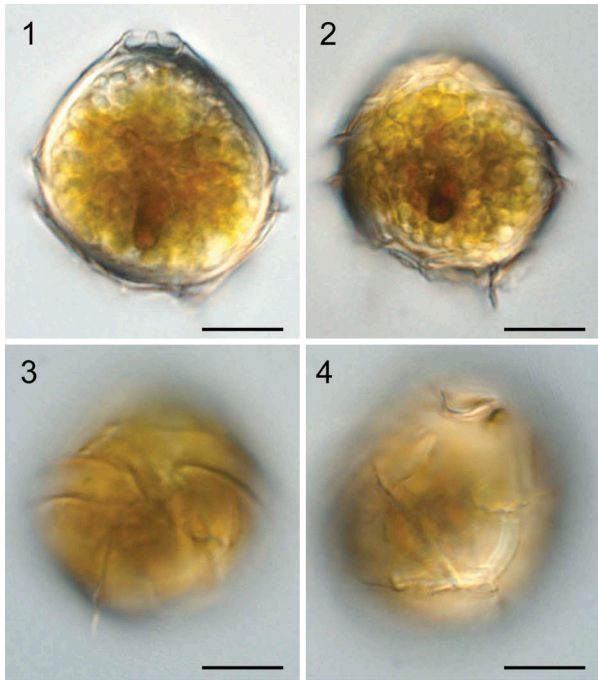
Figs 1–4. Light micrographs of live cysts of *Bysmatrum subsalsum* from France. Fig. 1. Ventral view in mid-focus showing numerous granules, a red accumulation body and the apical stalk. Fig. 2. Dorsal view showing numerous granules and a red accumulation body. Fig. 3. Ventral view showing the cingulum displacement. Fig. 4. Dorsal view showing the plates. Scale = 10 μm.

showed a plate formula of Po, cp, X, 4′, 3a, 7″, 6C, 4S, 5‴, 2⁗. The thecal plates were thick and covered with strong reticulations throughout (Figs 5–10). Thecal pores with a diameter of 0.14–0.28 μm were often observed along the plate margins. There were four apical plates. Plate 1′ was five-sided and asymmetrical with shorter anterior sutures than the posterior ones (Fig. 5). There were three anterior intercalary plates (1a, 2a and 3a), of which 3a is separated from 2a and 1a. Plate 1a was elongated rectangular whereas plates 2a and 3a were hexagonal and pentagonal, respectively (Figs 5–8). The length (of the upper side of 1a) and width (of the right side of 1a) ratio of the French strain TIO406 was 1.2–3.5 (mean =1.9±0.6, n=16). Occasionally, plate 1a was pentagonal (3 out of 37 cells). Plate 1″ was five-sided and the upper and lower side length ratio was 0.63–0.84 (mean =0.74±0.07, n=14). The cingulum was deeply excavated, around 3.5–4.2 μm wide (mean = 3.8±0.3 μm, n=20) and descending to about its own width, comprising six plates. The first three cingular plates (C1, C2 and C3) were similar in size and much smaller than the other three plates (Figs 5–7). The apical pore complex (APC) was tear-shaped comprising a pore plate (Po) with a much smaller, round cover plate (cp) and an elongated pentagonal canal plate (X) with thick margins formed by the raised borders of the apical plates (Figs 8, 9). The APC ranged

Figs 5–10. Scanning electron micrographs of cysts of French *Bysmatrum subsalsum*. Fig. 5. Ventral view showing the first apical plate and cingulum displacement. Fig. 6. Left lateral view showing the first three cingular plates (C1, C2 and C3). Fig. 7. Dorsal view showing the separation of plates 2a and 3a. Fig. 8. Apical view showing four apical plates (1′–4′), three anterior intercalary (1a, 2a and 3a) plates and seven precingular plates (1″–7″). Fig. 9. Apical pore complex showing the apical stalk emerging from the apical pore, pore plate (Po) and the narrow canal plate (X). Fig. 10. Antapical view showing five postcingular plates (1‴–5‴) and two antapical plates (1⁗, 2⁗) of unequal size. Scale = 10 μm.
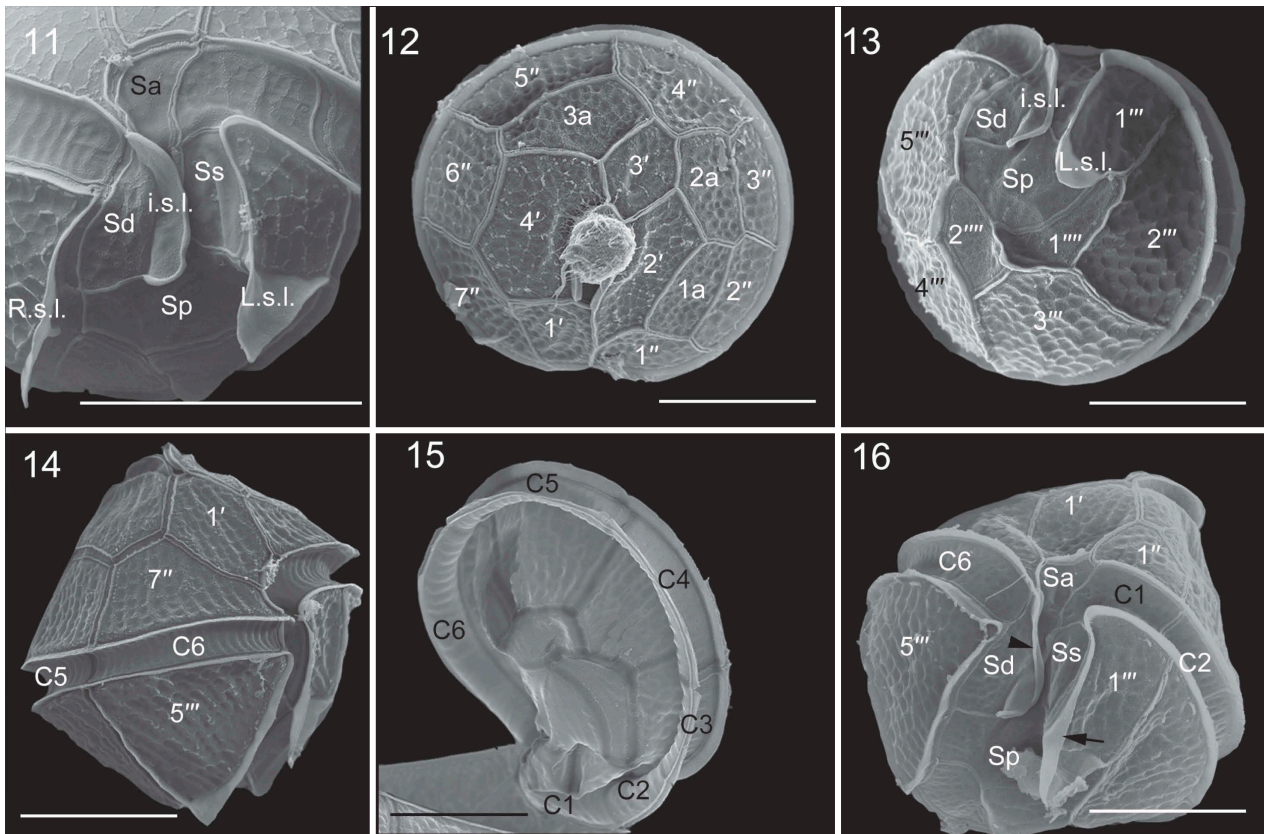
Figs 11–16. Scanning electron micrographs of vegetative cells of *Bysmatrum subsalsum* from French strain TIO406 (11) and Malaysian strain TBBYS02 (12–16). Fig. 11. The sulcus showing the anterior sulcal plate (Sa), left sulcal plate (Ss), right sulcal plate (Sd), posterior sulcal plate (Sp), the right sulcal list (R.s.l.), the left sulcal list (L.s.l.) and the internal sulcal list (i.s.l.). Fig. 12. Apical view showing four apical plates (1′–4′), three anterior intercalary (1a, 2a and 3a) plates and seven precingular plates (1″–7″). Fig. 13. Antapical view showing five postcingular plates (1‴–5‴) and left and internal sulcal lists. Fig. 14. Right lateral view showing the first apical plate. Fig. 15. Internal view showing six cingular plates (C1–C6). Fig. 16. Ventral view showing Sa, Ss, Sd, Sp plates, and L.s.l. (arrow), i.s.l. (arrowhead). Scale = 10 μm.

from 7.5 to 8.8 μm (mean =8.2±0.6, n=4) in length and from 3.2 to 3.5 μm (mean =3.4±0.1, n=4) in width. An apical stalk was sometimes observed protruding from the apical pore (Fig. 9). The first postcingular plate (1‴) was much smaller than the other plates in the series plates and bore a sulcal list, as well as the 5‴ (Fig. 10). The first antapical plate (1⁗) was elongated and narrow, displaced to the left, whereas the second antapical plate (2⁗) was pentagonal (Fig. 10). The anterior sulcal plate (Sa) and left sulcal (Ss) were elongated and narrow. The right sulcal (Sd) was triangular, with the internal sulcal list (i.s.l.) emerging from its left side. The posterior sulcal plate (Sp) was much wider than long. The left sulcal list (L.s.l.) emerged from the lower side of plate 1‴ and the right sulcal list (R.s.l.) covered the entire left side of plate 5‴ (Fig. 11).

The morphologies of Malaysian strains TBBYS02 (Figs 12–16) and TBBYS03 (Supplementary figs S1–S6) were similar to the French strains (Table 2), although the Malaysian strains lacked a high sulcal list on 5‴ (Figs 13, 16, Supplementary figs S1, S5) and possessed a more elongated 1a plate. The length and width ratio of the 1a plate were 1.8–4.0 (mean =2.5±0.7, n=14) and 1.8–4.8 (mean =3.4±0.9, n=15) for strains TBBYS02 and

TBBYS03. The length of the upper and lower side ratio of plate 1″ was 0.69–0.90 (mean =0.83±0.06, n=13) and 0.60–0.82 (mean =0.74±0.06, n=14) for strains TBBYS02 and TBBYS03.

Under LM, Malaysian strains showed a lot of banded chloroplasts in the periphery of the cells ('c' in Fig. 17). One pronounced orange eyespot was seen in the sulcal area (Fig. 18). The nucleus was large, elongated and located posteriorly ('n' in Figs 19, 20). TEM confirmed the presence of an eyespot in the sulcal area, and a posterior nucleus as well (Fig. 21). The chloroplasts had terminal pyrenoids with lamellae intruding the pyrenoid (Fig. 22). The thylakoids were grouped in twos or threes to form lamellae. The eyespot was located within a chloroplast comprising two rows of lipid globules (around 50 in each row) with a diameter of 70–110 nm (Fig. 23). There was one row of brick-like crystals enveloped by a vesicle overlying the eyespot, varying in size from 110 nm long and 80 nm wide to 220 nm long and 140 nm wide (Fig. 24).

Bysmatrum gregarium: The cells of strain TIO316 from the South China Sea were 27.2–37.9 μm long (mean =31.0±3.1 μm, n=20) and 25.5–35.9

Table 2. Morphological comparisons of *Bysmatrum* strains examined in the present study with closely related species.
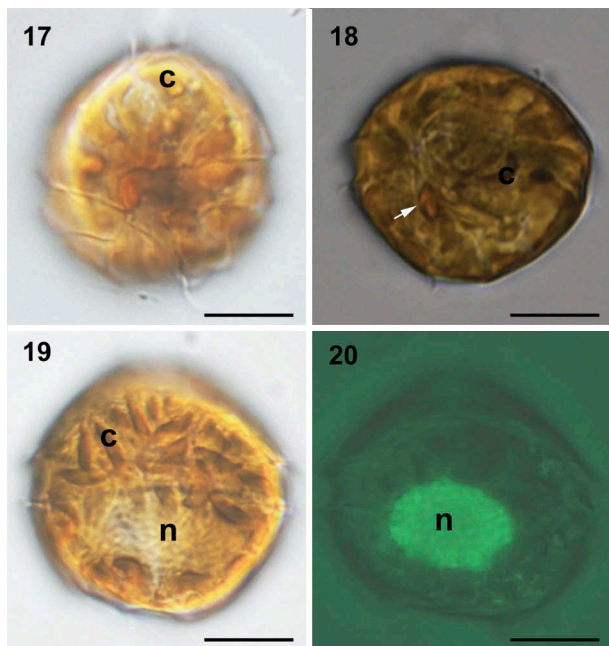
Species	*Bysmatrum subsalum*	*Bysmatrum subsalum*	*Bysmatrum subsalum*	*Bysmatrum subsalum*	*Bysmatrum subsalum*	*Bysmatrum subsalum*
Strains/origin	TBBYS02/SCS	TBBYS03/SCS	TIO406/French Atlantic	Aral Sea	Argentina	Florida, USA
Shape in ventral view	Pentagonal	Pentagonal	Pentagonal	Pentagonal	Pentagonal	Pentagonal
Shape in apical view	Oval, slightly dorsoventrally compressed	Oval, slightly dorsoventrally compressed	Oval, slightly dorsoventrally compressed	Oval, slightly dorsoventrally compressed	Oval, slightly dorsoventrally compressed	Oval, slightly dorsoventrally compressed
Apical stalk	Yes	Yes	Yes	NA	NA	NA
Nucleus	Elongated, hypothecal	Elongated, hypothecal	NA	NA	Rounded	Elongated, in the centre
Eyespot	Type B	Yes	NA	NA	NA	Yes
Thecal pore	Yes	Yes	Yes	NA	NA	NA
Thecal pore size (μm)	0.1–0.2	0.1–0.3	0.14–0.28	NA	NA	NA
SAPC	Teardrop	Teardrop	Teardrop	NA	NA	NA
APC length (μm)	7.5–8.8 (8.3, n=7)	6.7–9.1 (7.8, n=16)	7.5–8.8 (8.2, n=4)	NA	NA	NA
APC width (μm)	3.4–4.5 (3.9, n=7)	3.0–4.0 (3.4, n=16)	3.2–3.5 (3.4, n=4)	NA	NA	NA
Cell length (μm)	26.0–34.8	26.5–36.5	22.7–31.7	40–46	22.5–32	23.5–41
Cell width (μm)	24.7–31.4	22.0–29.4	26.0–36.9	38–44	16–29	21–51
Length: width ratio	1.0–1.2	0.9–1.2	1.1–1.2	NA	NA	NA
1st apical plate	Pentagonal	Pentagonal	Pentagonal	Pentagonal	Pentagonal	Pentagonal
1a morphology	Elongated rectangular	Elongated rectangular	Elongated rectangular	Elongated rectangular	Elongated rectangular	Pentagonal (rectangular)
L / W of 1a	1.8–4.0 (2.5, n=14)	1.8–4.8 (3.4, n=14)	1.2–3.5 (1.9, n=16)	1.8	2.7	NA
2a morphology	Hexagonal	Hexagonal	Hexagonal	Pentagonal	Hexagonal	Pentagonal (hexagonal)
3a morphology	Pentagonal	Pentagonal	Pentagonal	Pentagonal	Pentagonal	Pentagonal
Length of upper : lower side of 2''	0.69–0.90 (0.83, n=13)	0.60–0.82 (0.74, n=14)	0.63–0.84 (0.74, n=14)	0.75	0.63	0.7
Cingulum width (μm)	3.3–4.39(3.8, n=20)	2.9–4.2(3.6, n=20)	3.5–4.2(3.8, n=20)	NA	NA	3.0–5.0
Cingulum displacement	1	1	1	1	1	1
Sulcal list	2	2	3	3	3	3
Plate ornamentations	Reticulated	Reticulated	Reticulated	Reticulated	Reticulated	Reticulated
Cyst production	NA	NA	yes	yes	NA	NA
Cyst shape	NA	NA	Ovoid maintaining theca	NA	NA	NA
Cyst size (μm)	NA	NA	L: 30.0–40.9; W: 26.9–34.3	NA	NA	NA
Reference	Present study	Present study	Present study	Ostenfeld 1908	Balech 1964	Steidinger & Balech 1977

Species	*Bysmatrum subsalum*	*Bysmatrum subsalum*	*Bysmatrum subsalum*	*Bysmatrum gregarium*	*Bysmatrum granulosum*	*Bysmatrum granulosum*
Strains/origin	East China Sea / Caribbean Sea	East Mediterranean Sea	West Mediterranean Sea	TIO316/SCS	SP004/SCS	A10-P14-R2/SCS
Shape in ventral view	Pentagonal	Pentagonal/ovoid	Pentagonal/ovoid	Pentagonal	Pentagonal	Pentagonal
Shape in apical view	Oval, dorsoventrally compressed	Oval, slightly dorsoventrally compressed	Oval, slightly dorsoventrally compressed	Oval, slightly	Pentagonal dorsoventrally compressed	Oval, dorsoventrally compressed
Apical stalk	NA	NA	Yes	NA	Yes	NA
Nucleus	NA	NA	Hypothecal	NA	Elongated, in the centre	NA
Eyespot	NA	NA	Yes	Yes	NA	NA
Thecal pore	NA	NA	Yes	Yes	Yes	Yes
Thecal pore size (μm)	NA	NA	0.03–0.09 for smaller pores, 0.10–0.20 for larger ones	0.19–0.31	0.14–0.28	0.14–0.28
SAPC	NA	Teardrop?	Teardrop/polygonal	Teardrop	Polygonal	Polygonal
APC length (μm)	6.5	NA	3.7–10.8 (7.2, n=72)	5.5–6.7 (6.2)	5.3–8.9 (6.9)	5.1–9.8 (7.4)
APC width (μm)	2.3	NA	2.5–7.4 (4.7, n=72)	2.1–3.1 (2.8)	1.4–3.5 (2.6)	2.1–4.3 (2.8)

(*Continued*)

Table 2. (Continued).

Species	Bysmatrum subsalum	Bysmatrum subsalum	Bysmatrum subsalum	Bysmatrum gregarium	Bysmatrum granulosum	Bysmatrum granulosum
Cell length (μm)	32–41	21–45	22.3–50	24.9–37.9	36.4–42.8	37.7–55.4
Cell width (μm)	28–37	23–47	19.8–50	25.5–35.9	30.2–42.6	34.8–51.5
Length: width ratio	NA	NA	0.9–1.3	0.9–1.1	1.0–1.1	1.0–1.1
1st apical plate	Pentagonal	Pentagonal	Pentagonal	Pentagonal	Pentagonal	Pentagonal
1a morphology	Elongated rectangular	Elongated rectangular	Elongated rectangular	Trapezoid	Rectangular	Rectangular/penta
Length: width ratio of 1a (average)	1.6	2.5	1.9–4.8	0.9–4.0 (1.9, n=9)	1.1–2.3 (1.5, n=12)	1.8–4.0 (2.6, n=9)
2a morphology	Hexagonal	Hexagonal	Pentagonal	Hexagonal	Hexagonal	Pentagonal/hexagonal
3a morphology	Pentagonal	Pentagonal	Pentagonal	Pentagonal	Pentagonal	Pentagonal
Length of upper: lower side of 2″	0.67	0.73	0.81	0.45–0.57 (0.50, n=7)	0.65–0.85 (0.74, n=12)	0.63–0.84 (0.72, n=7)
Cingulum width (μm)	3	NA	1.9–6.2 (4.0)	2.7–3.4 (3.0)	2.3–4.4 (3.4)	1.5–3.8 (2.5)
Cingulum displacement	1	1	1–1.5	1.5	1.5	1.5
Sulcal list	2	2	3	2	2	2
Plate ornamentations	Reticulated	Reticulated	Reticulated	Reticulated	Wart-like projections	Wart-like projections
Cyst production	NA	Yes	Yes	NA	NA	NA
Cyst shape	NA	Rounded without theca	Ovoid maintaining theca (1st morphotype) and rounded without theca (2nd morphotype)	NA	NA	NA
Cyst size (μm)	NA	41–51 in diameter	L: 38.8–46.0, W: 38.7–44.4 for the 1st morphotype; 19.7–20.4 in diameter for the 2nd morphotype	NA	NA	NA
Reference	Faust 1996	Gottschling et al. 2012	Anglès et al. 2017	Present study	Present study	Present study

SCS: South China Sea; SAPC: Shape of apical pore complex (APC, Po + X plates); L / W of 1a: Length: width ratio of 1a (average); NA: not available.

Figs 17–20. Light micrographs of live cells of *Bysmatrum subsalsum* from Malaysian strains TBBYS02 (17–19) and TBBYS03 (20). Fig. 17. Ventral view showing the gross morphology and cingulum displacement. Fig. 18. Ventral view showing the banded chloroplasts (c) and a red eyespot in the sulcal area (arrow). Fig. 19. Dorsal view showing an elongated nucleus (n) and numerous chloroplasts (c). Fig. 20. Dorsal view showing an elongated nucleus (n) (Sybr Green staining). Scale = 10 μm.

μm wide (mean =31.1±2.7 μm, n=20). The cells had a conical epitheca and a rounded hypotheca (Figs 25, 26). *Bysmatrum gregarium* showed a plate formula of Po, cp, X, 4′, 3a, 7″, 6C, 4S, 5‴, 2⁗. The thecal plates were thick and covered with strong reticulations. Thecal pores were often observed on the plates.

The first apical plate (1′) was five-sided and asymmetrical with longer anterior sutures than the posterior ones (Fig. 25). There were three anterior intercalary plates (1a, 2a and 3a). Plate 1a was nearly square and 2a and 3a were hexagonal and pentagonal respectively (Figs 26, 27). The length (of the upper side of 1a) and width (of the right side of 1a) ratio was 0.9–4.0 (mean =1.9 ± 1.1, n=9). Plate 1″ was five-sided and the length of the upper and lower side ratio was 0.45–0.57 (mean =0.50±0.05, n=7). The cingulum was deeply excavated and descending to about 1.5 times its own width, comprising six plates of unequal size (Figs 25–27). The first three cingular plates (C1, C2 and C3) were similar in size and much smaller than the three other plates. The first postcingular plate (1‴) was much smaller than other plates in this series (Fig. 28). The first antapical plate (1⁗) was elongated and narrow, displaced to the left, whereas the second antapical plate (2⁗) was pentagonal (Fig. 28). The apical pore complex

comprised a round pore plate (Po), a round cover plate (cp) and an elongated canal plate (X) with a round apical pore located in the middle of the pore plate (Fig. 29).

There were four sulcal plates and two sulcal lists. The anterior sulcal plate (Sa) was elongated and narrow. The left sulcal (Ss) was elongated and narrow too. The right sulcal (Sd) was fan-shaped, with a small internal sulcal list (i.s.l.) at its left side. The posterior sulcal plate (Sp) was wider than long (Fig. 30). The left sulcal list (L.s.l.) emerged from the right of plate 1‴ (Fig. 28).

Bysmatrum granulosum: Cells of the strain SP004 from the South China Sea were 34.0–42.8 μm long (mean =38.8±2.5 μm, n=13) and 30.2–42.6 μm wide (mean =35.5±3.8 μm, n=18). The cells had a conical epitheca and a round hypotheca (Fig. 31). *Bysmatrum granulosum* showed a plate formula of Po, cp, X, 4′, 3a, 7″, 6C, 4S, 5‴, 2⁗. The thecal plates were thick and covered with small wart-like projections except on the sulcal and cingular plates (Figs 31–36). The apical pore complex was elongated comprising a pore plate (Po) and a narrow canal plate (X) with thickened margins formed by the raised borders of the apical plates (Fig. 34).

The first apical plate (1′) was five-sided and asymmetrical with anterior sutures equal in length to the posterior ones (Fig. 31). There were three anterior intercalary plates (1a, 2a and 3a). Plates 1a, 2a and 3a were rectangular, hexagonal and pentagonal respectively (Figs 32, 33). The length (of the upper side of 1a) and width (of the right side of 1a) ratio was 1.1–2.3 (mean =1.5±0.4, n=12). Plate 1″ was five-sided and the length of the upper and lower side ratio was 0.65–0.85 (mean =0.74±0.05, n=12). The cingulum was deeply excavated and descended about 1.5 times of own width, comprising six plates of unequal size (Figs 31, 33). The first three cingular plates (C1, C2 and C3) were similar in size and much smaller than the three other plates. The first postcingular plate (1‴) was smaller than other plates in this series (Fig. 35). The first antapical plate (1⁗) was wider than long, displaced to the left, whereas the second antapical plate (2⁗) was five-sided and slightly larger (Fig. 35).

There were four sulcal plates and two sulcal lists. The anterior sulcal plate (Sa) was triangular and the left sulcal (Ss) and right sulcal (Sd) were elongated and narrow. A small internal sulcal list (i.s.l.) was located at the left side of Sd. The posterior sulcal plate (Sp) was wider than long (Fig. 36). The left sulcal list (L.s.l.) emerged from the right side of plate 1‴ (Fig. 35).

Cells of strain A10-P14-R2 from the South China Sea were 37.7–55.4 μm long (mean =46.2 ±4.2 μm, n=40) and 34.8–50.3 μm wide (mean
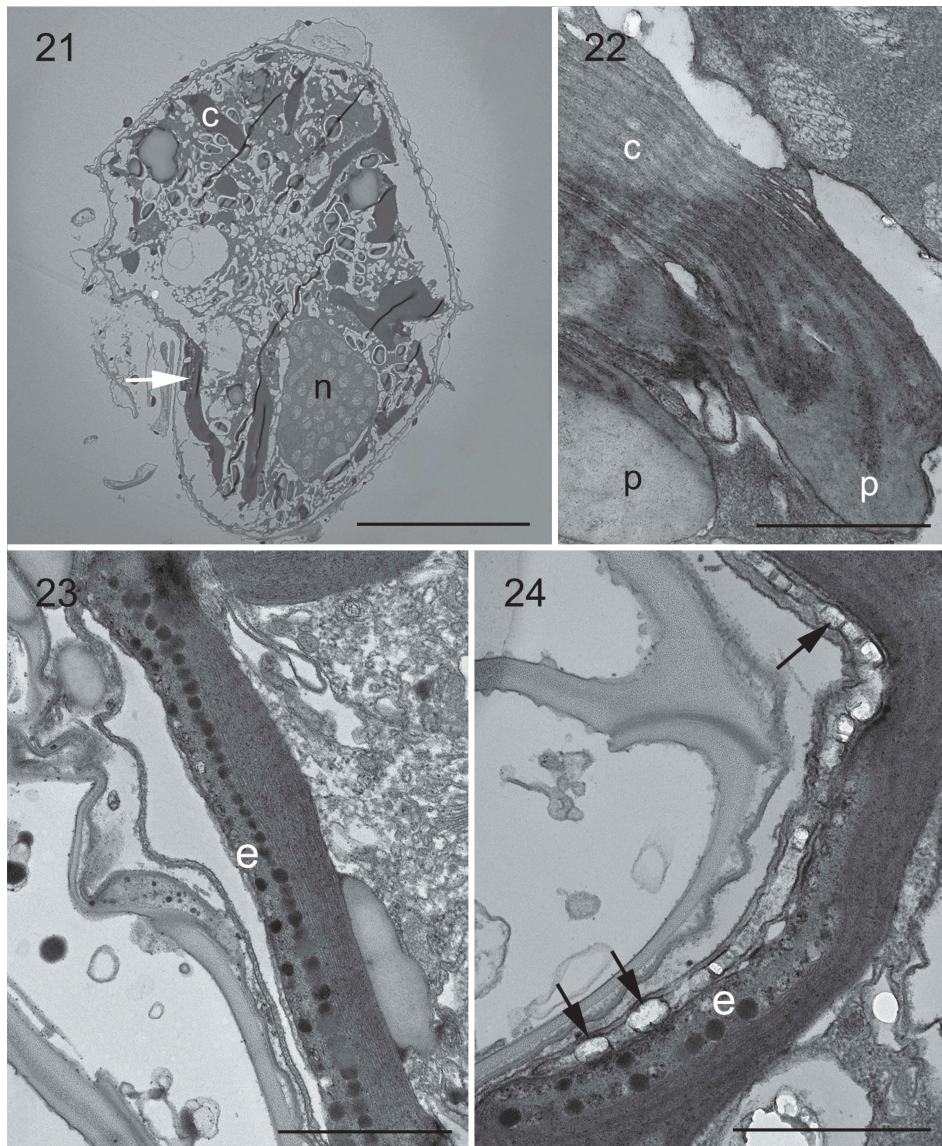
Figs 21–24. Transmission electron micrographs of vegetative cells of *Bysmatrum subsalsum* strain TBBYS02. Fig. 21. A longitudinal section through the cell showing a nucleus (n), several chloroplasts (c) and an eyespot (arrow). Fig. 22. Several chloroplasts (c) with terminal pyrenoids (p). Fig. 23. An eyespot (e) comprising two rows of lipid globules located within a chloroplast nearby sulcus. Fig. 24. Detail of the eyespot showing one row of overlying brick-like crystals (arrows). Scale: Fig. 21 = 10 μm; Figs 22–24 = 1 μm.

=43.3±4.1 μm, n=40). The cells shared similar morphology with strain SP004 (Supplementary figs S7–S12, Table 2).

Epithecal plate overlap in Bysmatrum, Parvodinium and Vulcanodinium

The epithecal plate overlap of all studied *Bysmatrum* species is identical and is exemplified in *B. subsalsum* (Fig. 37). The epithecal plate overlap of *Vulcanodinium* Nézan & Chomérat, *Parvodinium* Carty and *Bysmatrum* is characteristic for each genus (Figs 38, 39). These morphological differences are concordant with the genetic distances between the genera (Fig. 40).

MicroFTIR analysis of cysts of Bysmatrum subsalsum from French Atlantic

The geochemical analysis of the cyst walls of three specimens (M3S11, M3S12, M10S3) is illustrated in Fig. 41. There were absorptions for OH stretching centred at ~3300 cm^{-1} as well as aliphatic CH stretching (2725 & 2850 cm^{-1}) and bending (1420 & 1370 cm^{-1}) (not delineated in Fig. 41). There were also absorptions that are characteristic for polysaccharides (Pandey 1999; Kačuráková & Wilson 2001), including 1640 cm^{-1} (C=O stretching), 1160 cm^{-1} (C-O-C asymmetric vibration), 1115 cm^{-1} (glucose ring stretching) and C-O stretching absorptions at 1060 cm^{-1}, 1040 cm^{-1} and 1030 cm^{-1}.

Overall, M3S11 and M10S3 showed the greatest similarity, including a shoulder at 1540 cm^{-1} that
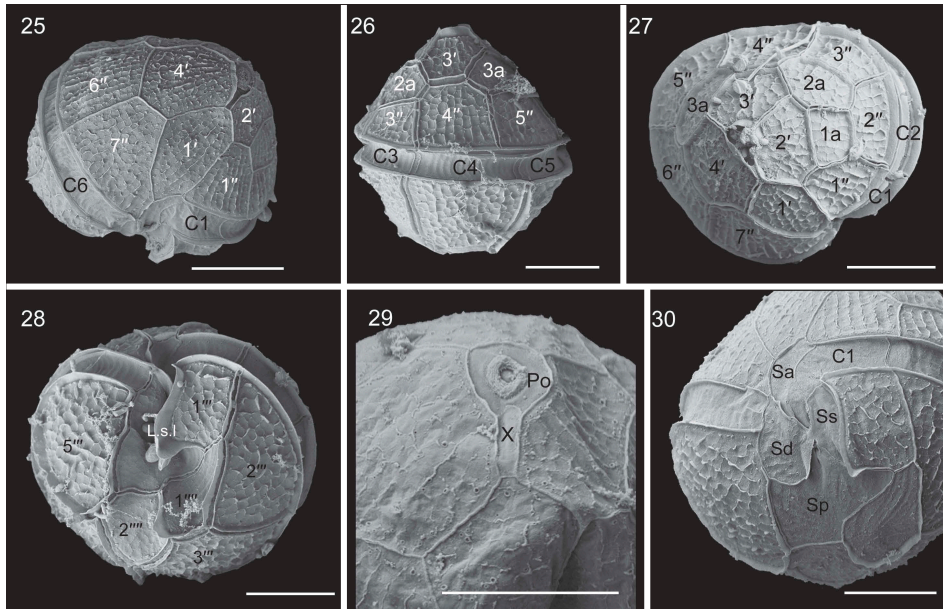
Figs 25–30. Scanning electron micrographs of vegetative cells of *Bysmatrum gregarium* strain TIO316. Fig. 25. Ventral view showing the first apical plate. Fig. 26. Dorsal view showing the cingulum plates. Fig. 27. Apical view showing four apical plates (1′–4′), three anterior intercalary (1a, 2a and 3a) plates and seven precingular plates (1″–7″). Fig. 28. Antapical view showing five postcingular plates (1‴–5‴), two antapical plates (1⁗, 2⁗) of unequal size and the left sulcal list (L.s.l.). Fig. 29. Apical pore complex showing the oval pore plate (Po), elongated canal plate (X) and round apical pore. Fig. 30. The sulcus showing an anterior sulcal plate (Sa), a right sulcal plate (Sd), a left sulcal plate (Ss), and a posterior sulcal plate (Sp). Scale = 10 μm.
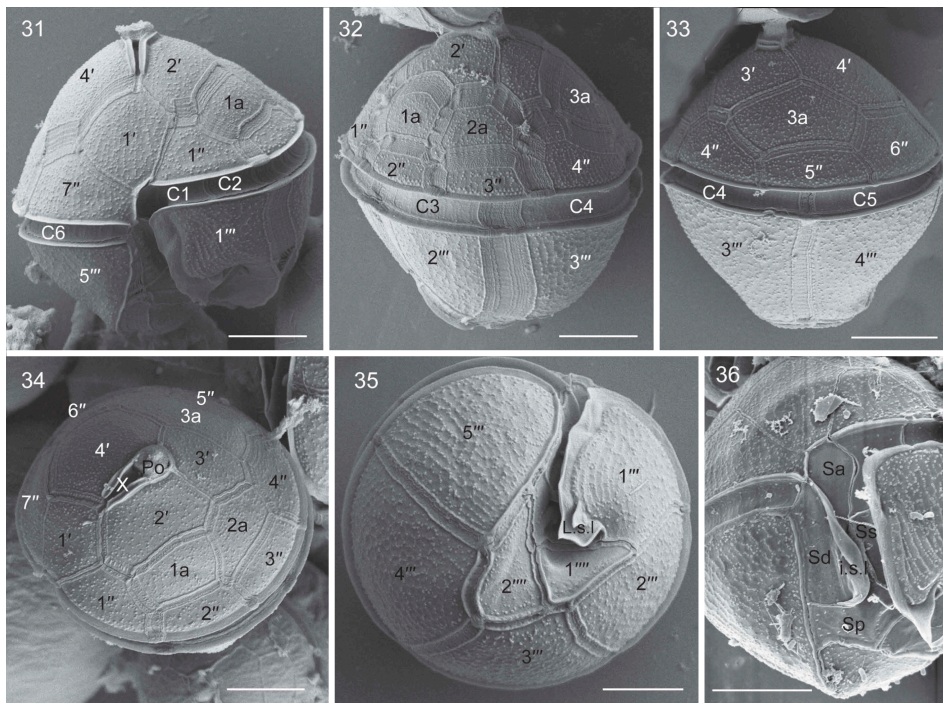
Figs 31–36. Scanning electron micrographs of vegetative cells of *Bysmatrum granulosum* strain SP004. Fig. 31. Ventral view showing the first apical plate (1′) and cingulum displacement. Fig. 32. Left lateral view showing the two anterior intercalary plates (1a, 2a). Fig. 33. Dorsal view showing the cingulum plates (C4, C5) and the third anterior intercalary plate (3a). Fig. 34. Apical view showing the apical pore complex, four apical plates (1′–4′), three anterior intercalary (1a, 2a and 3a) plates and seven precingular plates (1″–7″). Fig. 35. Antapical view showing five postcingular plates (1‴–5‴), two antapical plates (1⁗, 2⁗) of unequal size and the left sulcal list (L.s.l.). Fig. 36. The sulcus showing an anterior sulcal plate (Sa), a right sulcal plate (Sd), a left sulcal plate (Ss), a posterior sulcal plate (Sp), and the internal sulcal list (i.s.l.). Scale = 10 μm.
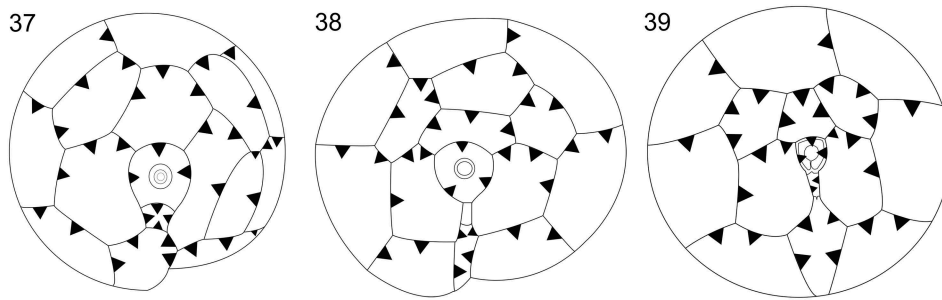
Figs 37–39. Plate overlaps of epitheca in *Bysmatrum, Vulcanodinium* and *Parvodinium*. Fig. 37. Plate overlaps of *Bysmatrum subsalsum*. Fig. 38. Plate overlaps of *Vulcanodinium rugosum*. Fig. 39. Plate overlaps of *Parvodinium umbonatum*.

could suggest either extracellular contamination or amide groups within the cyst wall; however, there were no other clear absorptions for proteinaceous material (see contamination discussion in Mertens *et al.*, 2015). The M3S12 spectrum is different in that it exhibits a shoulder at 1640 cm^{-1} and a band at 1590 cm^{-1} that reflect C=O and C=C stretching, respectively.

Molecular analysis and phylogeny

The genetic distance based on ITS1-5.8S-ITS2 sequences among *Bysmatrum* morphospecies ranged from 0.34 to 0.47 and those genetic distances at intraspecific level were 0.15 (*B. gregarium* and *B. granulosum*) and 0.09 to 0.41 (*B. subsalsum*) (Table 3).

The maximum likelihood (ML) and Bayesian inference (BI) analysis based on combined SSU rDNA, partial LSU rDNA and ITS sequences yielded similar phylogenetic trees. The BI tree is illustrated in Fig. 40. The genus *Bysmatrum* was monophyletic with maximal support. It was clearly nested within the Peridiniales and formed a clade with *Parvodinium, Peridiniopsis borgei, Palatinus apiculatus, Vulcanodinium rugosum, Peridinium cintum* and *Protoperidinium* with low support (68/0.71). *Bysmatrum subsalsum* consisted of two well-resolved subclades. One subclade comprised strains from the Mediterranean Sea (referred to ribotype A) and the other included strains from Malaysia and the French Atlantic (referred to ribotype B). *Bysmatrum gregarium* and *B. granulosum* grouped together with strong ML support (100), but low posterior probability (0.70).

Discussion

Morphology and biogeography

Bysmatrum subsalsum: The strains of *B. subsalsum* from the French Atlantic were characterized by the separation of plates 2a and 3a and an elongated rectangular 1a plate, thus fitting the original descriptions, especially the presence of three sulcal lists (Ostenfeld, 1908, fig. 50). Sulcal lists were also reported in specimens from Argentina (Balech, 1964, as *Peridinium subsalsum*), USA (Faust, 1996) and Mediterranean Sea (Gottschling *et al.*, 2012; Anglès *et al.*, 2017), but the right sulcal list was not present in the latter two reports or in the Malaysian strains TBBYS02 and TBBYS03 reported here. The shape of plate 1a is often rectangular in *B. subsalsum*, although a pentagonal 1a was occasionally observed (Faust & Steidinger, 1998; present study). The ratio of the length and width of 1a plate might be a useful indicator to differentiate *B. subsalsum* strains, but the ratio of the length of the upper and lower side of 2″ plate appears rather conservative among these strains (Table 2). A significant correlation between APC length and total cell length was reported in *B. subsalsum* from the Mediterranean Sea (Anglès *et al.*, 2017), and also confirmed in the Malaysian and French strains. Because of the morphological similarity between our strains and strains from elsewhere, we identified them as *B. subsalsum*.

Bysmatrum subsalsum has a worldwide distribution, being recorded in the Aral Sea (Ostenfeld, 1908), the Caribbean (Faust & Steidinger, 1998), the Gulf of Mexico (Limoges *et al.*, 2015), the Mediterranean Sea (Gottschling *et al.*, 2012; Anglès *et al.*, 2017), Argentina (Balech, 1964, as *P. subsalsum*), Japan (Horiguchi, 1983) and in the South China Sea and French Atlantic as reported here.

Bysmatrum subsalsum is morphologically close to *Peridinium sociale* (Henneguy) Biecheler as described by Biecheler (1952), but our strains are much smaller and have less cingulum displacement (1.0 versus 1.5 cingular widths). However, the Mediterranean *B. subsalsum* strains can have a cingulum displacement from 1.0 to 1.5 and have a large variability in cell size (Anglès *et al.*, 2017). Therefore, the species reported by Biecheler (1952) might be conspecific with *B. subsalsum*. However, whether *B. subsalsum* is a junior synonym of *Peridinium sociale* remains to determined since Henneguy (1890) described *Glenodinium sociale* without giving information about the tabulation.
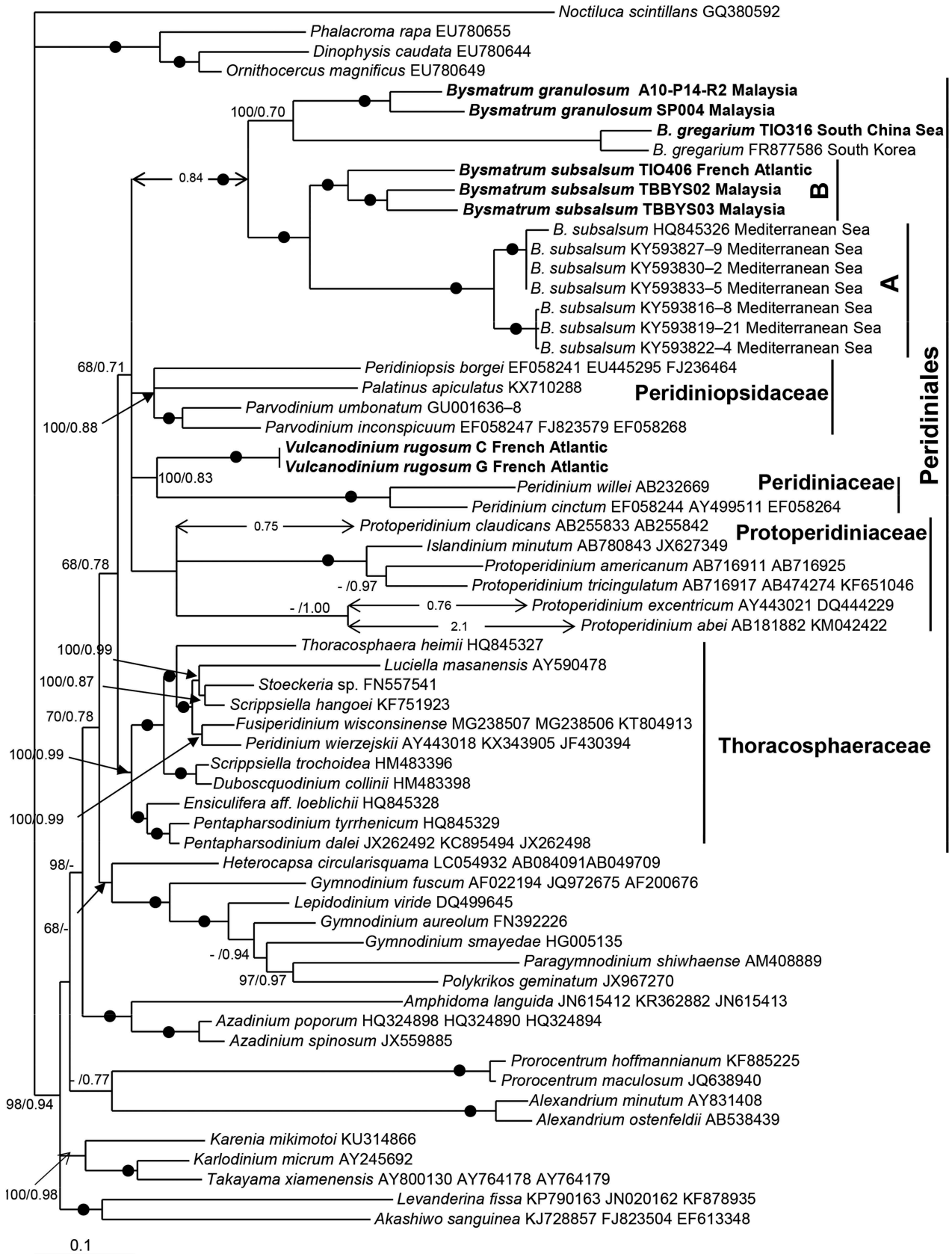
Fig. 40. Phylogeny of *Bysmatrum* inferred from concatenated SSU, partial LSU rDNA and ITS sequences using Bayesian inference . New sequences are indicated in bold. Branch lengths are drawn to scale, with the scale bar indicating the number of nucleotide substitutions per site. The long branches are reduced in size with their actual size indicated. Numbers on branches are statistical support values to clusters to the right of them (left: maximum likelihood bootstrap support values; right: Bayesian posterior probabilities). Black circles indicate maximal support (bootstrap = 100% in ML and pp = 1.00 in BI respectively).
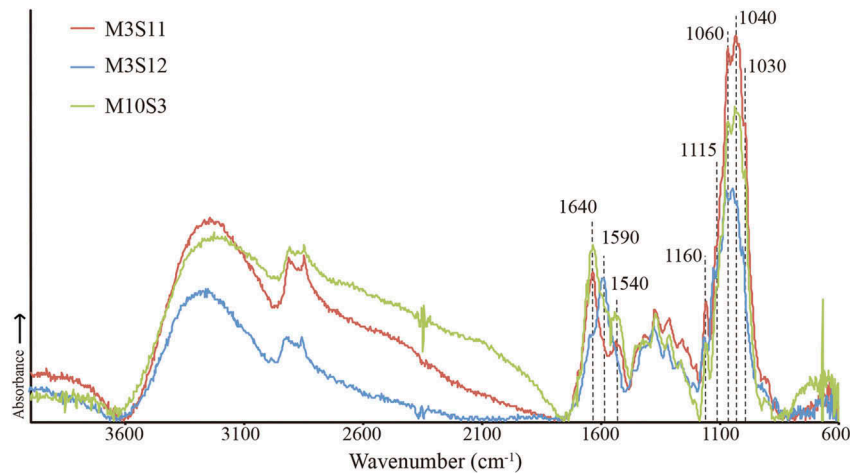
Fig. 41. Micro-Fourier transform infrared spectra of three *Bysmatrum subsalsum* cysts from France.

Table 3. Uncorrected pairwise distances among *Bysmatrum* species based on ITS sequences.

	B. subsalsum TBBYS02	B. subsalsum TBBYS03	B. subsalsum TIO406	B. subsalsum D323	B. subsalsum FB1	B. granulosum A10-P14-R2	B. granulosum SP004	B. gregarium TIO316	B. gregarium
B.subsalsum TBBYS02(SCS)	–								
B.subsalsum TBBYS03(SCS)	0.27	–							
B.subsalsum TIO406 (France)	0.30	0.33	–						
B.subsalsum D323(MED)	0.38	0.39	0.38	–					
B.subsalsum FB1 (MED)	0.35	0.36	0.36	0.09	–				
B. granulosum A10-P14-R2 (SCS)	0.40	0.41	0.41	0.42	0.43	–			
B. granulosum SP004(SCS)	0.38	0.39	0.40	0.41	0.40	0.15	–		
B. gregarium TIO316(SCS)	0.47	0.43	0.44	0.47	0.46	0.48	0.46	–	
B. gregarium (Korea)	0.45	0.44	0.46	0.45	0.44	0.48	0.46	0.15	–

SCS: South China Sea; MED: Mediterranean Sea.

An apical stalk emerged from the apical pore of *B. subsalsum* (Fig. 9), and has been reported for *B. arenicola* and *B. gregarium* as well, suggesting that this is a common feature for the genus, possibly related to their epibenthic life stage. Mucus excreted from the apical stalk was observed in *B. subsalsum* and *B. granulosum*, which could help them to attach to a substrate, such as macroalgal surfaces, as illustrated for *B. arenicola* by Horiguchi & Pienaar (1988*b*).

Cysts of *Bysmatrum subsalsum* from the French Atlantic are covered by thecal plates, as was reported for the Gulf of Mexico and Mediterranean Sea (Limoges *et al.*, 2015; Anglès *et al.*, 2017). The geochemical analysis of the cyst walls of three specimens (M3S11, M3S12, M10S3; Fig. 41) showed overall consistency with other extant dinoflagellate cysts analysed from surface sediments (e.g. Bogus *et al.*, 2014; Mertens *et al.*, 2015). The M3S12 spectrum

could indicate that aromatic bonds are present, similar to *Pyrodinium bahamense* (Mertens *et al.*, 2015). The variability among the three specimens could reflect intraspecific differences even in cysts from the same location. The spectra of *B. subsalsum* cysts did not resemble those from heterotrophic dinoflagellates (Bogus *et al.*, 2014), supporting that they have an autotrophic nutritional strategy.

Bysmatrum gregarium: Lombard & Capon (1971) described a new thecate dinoflagellate isolated from tidal pools in southern California and named it *Peridinium gregarium* Lombard & Capon. After the illegitimate renaming of *P. gregarium* as *Scrippsiella caponii* by Horiguchi & Pienaar (1988*a*), and its therefore illegitimate transfer to *Bysmatrum caponii* by Faust & Steidinger (1998), the correct name for this species is now considered to be *Bysmatrum gregarium* (see Hoppenrath *et al.*, 2014, for further details). The Chinese strain TIO316 generally fits

the original description of *B. gregarium* but differs in the relative size of C2 and C3 (similar size of C2 and C3 in TIO316 versus half length of C3 in the type material) (Horiguchi & Pienaar, 1988*a*). Strain TIO316 is morphologically indistinguishable from the Korean strains described by Jeong *et al.* (2012) which also have plates C2 and C3 of similar size. *Bysmatrum gregarium* is morphologically very close to *B. subsalsum* (Anglès *et al.*, 2017), however, the ratio of length of upper and lower sides of 2″ plate appears useful to differentiate them (0.5 vs 0.7, see Table 2). Additionally, the ratio of total cell length and APC length can reach 5.0 in *B. gregarium* strain TIO316, much larger than those of *B. subsalsum* strains (less than 4.0).

Bysmatrum gregarium has been reported in southern California, western Korea (Jeong *et al.*, 2012), the Mexican Caribbean (Almazán-Becerril *et al.*, 2015), Hawai'i (Parsons & Preskitt, 2007) and in the South China Sea (this study). This is also the first report of *Bysmatrum* in Chinese waters.

Bysmatrum granulosum: The Malaysian strains SP004 and A10-P14-R2 fit the original description having wart-like projections on the thecal surface. *Bysmatrum granulosum* was described from sediment and coral samples collected from Reunion Island, South West Indian Ocean (Ten-Hage *et al.*, 2001) and later found in Sabah, Malaysia (Mohammad-Noor *et al.*, 2007) and the Mexican Caribbean (Almazán-Becerril *et al.*, 2015). In this study, it was found in Rawa Island and Perhentian Island, extending its distribution to the Malay Peninsula. Our strains were also isolated from coral reef debris, supporting the idea that this species is always associated with corals (Ten-Hage *et al.*, 2001).

Eyespot structure of Bysmatrum subsalsum *from Malaysia*

Moestrup & Daugbjerg (2007) reviewed five different types of eyespot in dinoflagellates, excluding the complex ocelloid of the Warnowiaceae (Greuet, 1987): Type A, characterized by one to several layers of opaque globules inside a chloroplast; Type B, a vesicle containing crystal-like units overlying an eyespot type A-like chloroplast; Type C, layers of opaque lipid globules not bounded by a membrane; Type D, layers of opaque globules inside a reduced chloroplast; and Type E, several layers of crystal-like units contained in a vesicle. Craveiro *et al.* (2010) reported a new type of eyespot (as Type F), characterized by a single layer of vesicle-contained crystal-like units overlying layers of more or less fused globules not bounded by membranes. The eyespot of *B. subsalsum* is located within the chloroplast and consists of two rows of lipid globules with overlying brick-like crystals, thus was identified as a Type B eyespot, as also reported in

Borghiella dodgei (Moestrup *et al.*, 2008) and *Baldinia anauniensis* (Hansen *et al.*, 2007).

A prominent eyespot has been reported in *B. subsalsum* (Faust & Steidinger, 1998; Anglès *et al.*, 2017), *B. granulosum* (Ten-Hage *et al.*, 2001) and *B. gregarium* (Jeong *et al.*, 2012) and is confirmed here in *B. subsalsum*. However, it was not described for *B. arenicola* (Horiguchi & Pienaar, 1988*b*) or *B. teres* (Murray *et al.*, 2006). A Type A eyespot was reported in *B. austrafrum* (Dawut *et al.*, 2018), and in species of Peridiniales such as *Scrippsiella trochoidea* (Craveiro *et al.*, 2011), *Palatinus apiculatus* (Craveiro *et al.*, 2009), *Naiadinium polonicum* (Craveiro *et al.*, 2015) and *Peridinium willei* (Moestrup & Daugbjerg, 2007), suggesting that *Bysmatrum* is systematically distant from Thoracosphaeraceae but close to Peridiniaceae and Peridiniopsidaceae (Fig. 40).

Phylogeny and genetic differentiation

The phylogenetic position of *Bysmatrum* was first reported by Gottschling *et al.* (2012) using concatenated SSU, ITS and LSU sequences. In their trees, *Bysmatrum subsalsum* appears distant from other Peridiniales, and this led Gottschling *et al.* (2012) to suggest that *Bysmatrum* is closer to Gonyaucales. Later however, Jeong *et al.* (2012) reported that *Bysmatrum gregarium* is close to *Protoperidinium* and *Peridinium* based on SSU and LSU rDNA sequences. The phylogenetic tree based on SSU, partial LSU rDNA and ITS (Fig. 40) supports the nesting of *Bysmatrum* within the Peridiniales (Anglès *et al.*, 2017) and a close relationship between *Bysmatrum* and the freshwater planktonic genus *Parvodinium*. These two genera share the separation of anterior intercalary plates (Carty, 2008), although *Parvodinium* only has two anterior intercalary plates in contrast to the three found in *Bysmatrum* (Hansen & Flaim, 2007; Carty, 2008). *Parvodinium* was classified in the family Peridiniopsidaceae together with *Peridiniopsis* Bourrelly and *Palatinus* Craveiro, Calado, Daugbjerg & Moestrup (Gottschling *et al.*, 2017). An eyespot is probably present in *Parvodinium inconspicuum* (Lemmermann) Carty (Carty, 2008), but detailed study has not been carried out and should be the focus of future research.

The close relationship between *Bysmatrum* and *Vulcanodinium* is not surprising because of their similarity in shape and plate pattern and thick, reticulate plates. The major difference is the separation of plates 2a and 3a in *Bysmatrum*, which does not occur in *Vulcanodinium* (Nézan & Chomérat, 2011). In addition, *Bysmatrum subsalsum* strain TBBYS02 is not able to produce pinnatoxin (Krock, B. personal communication) while *Vulcanodinium rugosum* is always toxic (Selwood *et al.*, 2014). The ITS-based genetic distances at intraspecific level in *B. subsalsum*

reached 0.4, similar to those between the different sequenced *Bysmatrum* species (Table 3) and much greater than the threshold of 0.04 used to delimit species based on ITS based genetic distances (Litaker *et al.*, 2007), supporting the idea that there is cryptic diversity within *B. subsalsum* (Anglès *et al.*, 2017). It is worth noting that two Malaysian strains of *B. subsalsum* were recovered from a single water sample and showed large genetic differentiation, as also reported in the two *B. granulosum* strains collected in neighbouring locations. Whether such genetic differentiations also occurs in other *Bysmatrum* species remains to be confirmed.

Acknowledgements

Disclosure statement

Funding

Author contributions

Z. Luo: electron microscopy and drafting manuscript; Z.F. Lim: culture experiments; K.N. Mertens: original concept, drafting and editing manuscript, light microscopy, scanning electron microscopy; P. Gurdebeke:drafting and editing manuscript, interpretation of FTIR spectra; K. Bogus: drafting and editing manuscript, interpretation of FTIR spectra; M. C. Carbonell-moore: drafting and editing manuscript, interpretation of SEM images, illustration; H. Vrielinck: drafting and editing manuscript, interpretation of FTIR spectra; C.P. Leaw: analysis of molecular data; P.T. Lim: analysis of molecular data; N. Chomérat: drafting and editing manuscript, scanning electron microscopy; X. Li: culture experiment; H. Gu: original concept and editing of manuscript.

Supplementary information

The following supplementary material is accessible via the Supplementary Content tab on the article's online page at http://10.1080/09670262.2018.1449014
Supplementary table S1. GenBank accession numbers of strains or isolates examined in the present study.

Supplementary figs S1–S6. Scanning electron micrographs of vegetative cells of *Bysmatrum subsalsum* from Malaysian strain TBBYS03. **Fig. S1**. Left lateral view showing the elongated 1a plate and three cingular plates (C1–C3). **Fig. S2**. Apical view showing four apical plates (1′–4′), three anterior intercalary (1a, 2a and 3a) plates and seven precingular plates (1″–7″). **Fig. S3**. Dorsal view showing three anterior intercalary (1a, 2a and 3a) plates. **Fig. S4**. Ventral view showing five postcingular plates (1‴–5‴) and two antapical plates (1⁗, 2⁗) of unequal size. **Fig. S5**. The sulcus showing the anterior sulcal plate (Sa), left sulcal plate (Ss), right sulcal plate (Sd), posterior sulcal plate (Sp), the left sulcal list (L.s.l.) and the internal sulcal list (i.s.l.). **Fig. S6**. Antapical view showing five postcingular plates (1‴–5‴) and two antapical plates (1⁗, 2⁗) of unequal size. Scale bars = 10 µm.
Supplementary figs S7–S12. Scanning electron micrographs of vegetative cells of *Bysmatrum granulosum* strain A10-P14-R2. **Fig. S7**. Ventral view showing the first apical plate and cingulum displacement. **Fig. S8**. Left lateral view showing the two anterior intercalary plates (1a, 2a). **Fig. S9**. Dorsal view showing the cingulum plates and the third anterior intercalary plate (3a). **Fig. S10**. Apical view showing the apical pore complex, four apical plates (1′–4′), three anterior intercalary (1a, 2a and 3a) plates and seven precingular plates (1″–7″). **Fig. S11**. Antapical view showing five postcingular plates (1‴–5‴), two antapical plates (1⁗, 2⁗) of unequal size and the left sulcal list (L.s.l.). **Fig. S12**. The sulcus showing an anterior sulcal plate (Sa), a right sulcal plate (Sd), a left sulcal plate (Ss) and a posterior sulcal plate (Sp). Scale bars = 10 µm.

References

Adachi, M., Sako, Y. & Ishida Y. (1996). Analysis of *Alexandrium* (Dinophyceae) species using sequences of the 5.8S ribosomal DNA and internal transcribed spacer regions. *Journal of Phycology*, **32**: 424–432.

Almazán-Becerril, A., Escobar-Morales, S., Rosiles-González, G. & Valadez, F. (2015). Benthic-epiphytic dinoflagellates from the northern portion of the Mesoamerican Reef System. *Botanica Marina*, **58**: 115–128.

Anglès, S., Reñé, A., Garcés, E., Lugliè, A., Sechi, N., Camp, J. & Satta, C.T. (2017). Morphological and molecular characterization of *Bysmatrum subsalsum* (Dinophyceae) from the western Mediterranean Sea reveals the existence of cryptic species. *Journal of Phycology*, **53**: 833–847.

Balech, E. (1964). Tercera contribucion al conocimiento del genero *Peridinium*. *Museo Argentino de ciencias naturales 'Bernadino Rivadavia'e Instituto nacional de investigacion de las ciencias naturales, Revista, Hydrobiologia*, **4**: 179–195.

Balech, E. (1980). On the thecal morphology of dinoflagellates with special emphasis on circular and sulcal plates. *Anales del Centro de Ciencias del Mar y Limnologia, Universidad Nacional Autonomia de Mexico*, **7**: 57–68.

Biecheler, B. (1952). Recherches sur les Peridiniens. *Bulletin biologique de la France et de la Belgique*, **36**: 1–147.

Boc, A., Diallo, A.B. & Makarenkov, V. (2012). T-REX: a web server for inferring, validating and visualizing phylogenetic trees and networks. *Nucleic Acids Research*, **40**: W573–W579.

Bogus, K., Mertens, K.N., Lauwaert, J., Harding, I.C., Vrielinck, H., Zonneveld, K.A. & Versteegh, G.J. (2014). Differences in the chemical composition of

organic-walled dinoflagellate resting cysts from phototrophic and heterotrophic dinoflagellates. *Journal of Phycology*, **50**: 254–266.

Carty, S. (2008). *Parvodinium* gen. nov. for the Umbonatum group of *Peridinium* (Dinophyceae). *Ohio Journal of Science*, **108**: 103–107.

Craveiro, S., Calado, A.J., Daugbjerg, N. & Moestrup, Ø. (2009). Ultrastructure and LSU rDNA-based revision of *Peridinium* group palatinum (Dinophyceae) with the description of *Palatinus* gen. nov. *Journal of Phycology*, **45**: 1175–1194.

Craveiro, S.C., Moestrup, Ø., Daugbjerg, N. & Calado, A.J. (2010). Ultrastructure and large subunit rDNA-based phylogeny of *Sphaerodinium cracoviense*, an unusual freshwater dinoflagellate with a novel type of eyespot. *Journal of Eukaryotic Microbiology*, **57**: 568–585.

Craveiro, S.C., Calado, A.J., Daugbjerg, N., Hansen, G. & Moestrup, Ø. (2011). Ultrastructure and LSU rDNA-based phylogeny of *Peridinium lomnickii* and description of *Chimonodinium* gen. nov. (Dinophyceae). *Protist*, **162**: 590–615.

Craveiro, S.C., Daugbjerg, N., Moestrup, Ø. & Calado, A.J. (2015). Fine-structural characterization and phylogeny of *Peridinium polonicum*, type species of the recently described genus *Naiadinium* (Dinophyceae). *European Journal of Protistology*, **51**: 259–279.

Daugbjerg, N., Hansen, G., Larsen, J. & Moestrup, Ø. (2000). Phylogeny of some of the major genera of dinoflagellates based on ultrastructure and partial LSU rDNA sequence data, including the erection of three new genera of unarmoured dinoflagellates. *Phycologia*, **39**: 302–317.

Dawut, M., Sym, S.D., Suda, S. & Horiguchi, T. (2018). *Bysmatrum austrafrum* sp. nov. (Dinophyceae), a novel tidal pool dinoflagellate from South Africa. *Phycologia*, **57**: 169–178.

Faust, M.A. (1996). Morphology and ecology of the marine benthic dinoflagellate *Scrippsiella subsalsa* (Dinophyceae). *Journal of Phycology*, **32**: 669–675.

Faust, M.A. & Steidinger, K.A. (1998). *Bysmatrum* gen. nov. (Dinophyceae) and three new combinations for benthic scrippsielloid species. *Phycologia*, **37**: 47–52.

Fensome, R.A., Taylor, F.J.R., Norris, G., Sarjeant, W.A.S., Wharton, D.I. & Williams, G.L. (1993). A classification of fossil and living dinoflagellates. *Micropaleontology Special Publication*, **7**: 1–245.

Fritz, L. & Triemer, R. (1985). A rapid simple technique utilizing calcofluor white M2R for the visualization of dinoflagellate thecal plates. *Journal of Phycology*, **21**: 662–664.

Greuet, C. (1987). Complex organelles. In *The Biology of Dinoflagellates* (Taylor, F.J.R., editor), 117–142. Blackwell, Oxford.

Gottschling, M., Soehner, S., Zinssmeister, C., John, U., Plötner, J., Schweikert, M., Aligizaki, K. & Elbrächter, M. (2012). Delimitation of the Thoracosphaeraceae (Dinophyceae), including the calcareous dinoflagellates, based on large amounts of ribosomal RNA sequence data. *Protist*, **163**: 15–24.

Gottschling, M., Kretschmann, J. & Čalasan, A.Ž. (2017). Description of Peridiniopsidaceae, fam. nov. (Peridiniales, Dinophyceae). *Phytotaxa*, **299**: 293–296.

Gu, H., Luo, Z., Mertens, K.N., Price, A.M., Turner, R.E. & Rabalais, N.N. (2015a). Cyst-motile stage relationship, morphology, ultrastructure, and molecular phylogeny of the gymnodinioid dinoflagellate *Barrufeta resplendens* comb. nov., formerly known as *Gyrodinium resplendens*, isolated from the Gulf of Mexico. *Journal of Phycology*, **51**: 990–999.

Gu, H., Liu, T. & Mertens, K. (2015b). cyst-theca relationship and phylogenetic positions of *Protoperidinium* (Peridiniales, Dinophyceae) species of the sections Conica and Tabulata, with description of *Protoperidinium shanghaiense* sp. nov. *Phycologia*, **54**: 49–66.

Guillard, R.R.L. & Ryther, J.H. (1962). Studies of marine planktonic diatoms. I. *Cyclotella Nana* Hustedt and *Detonula confervacea* Cleve. *Canadian Journal of Microbiology*, **8**: 229–239.

Hall, T.A. (1999). BioEdit: a user-friendly biological sequence alignment editor and analysis program for Windows 95/98/NT, pp. 95–98.

Hansen, G., Daugbjerg, N. & Henriksen, P. (2007). *Baldinia anauniensis* gen. et sp. nov.: a "new" dinoflagellate from Lake Tovel, N. Italy. *Phycologia*, **46**: 86–108.

Hansen, G. & Flaim, G. (2007). Dinoflagellates of the Trentino Province, Italy. *Journal of Limnology*, **66**: 107–141.

Head, M.J. (1996). Modern dinoflagellate cysts and their biological affinities. In *Palynology: principles and applications* (Jansonius, J. & McGregor, D.C., editors), 1197–1248. American Association of Stratigraphic Palynologists Foundation, Dallas.

Henneguy, M.F. (1890). Contributions a l'étude de la faune des marais salants. *Compte Rendu Societé Biologique*, **9**: 625–627.

Hoppenrath, M., Murray, S.A., Chomérat, N. & Horiguchi, T. (2014). *Marine benthic dinoflagellates – unveiling their worldwide biodiversity*. Kleine Senckenberg-Reihe 54, Schweizerbart Science, Stuttgart.

Horiguchi, T. (1983). Life history and taxonomy of benthic dinoflagellates (Pyrrophyta). PhD thesis. University of Tsukuba, Tsukuba, Japan. 142 pp.

Horiguchi, T. & Pienaar, R.N. (1988a). A redescription of the tidal pool dinoflagellate *Peridinium gregarium* based on re-examination of the type material. *European Journal of Phycology*, **23**: 33–39.

Horiguchi, T. & Pienaar, R. (1988b). Ultrastructure of a new sand-dwelling dinoflagellate, *Scrippsiella arenicola* sp. nov. *Journal of Phycology*, **24**: 426–438.

Jeong, H.J., Jang, S.H., Kang, N.S., Yoo, Y.D., Kim, M.J., Lee, K.H., Yoon, E.Y., Potvin, É., Hwang, Y.J. & Kim, J.I. (2012). Molecular characterization and morphology of the photosynthetic dinoflagellate *Bysmatrum caponii* from two solar saltons in western Korea. *Ocean Science Journal*, **47**: 1–18.

Kačuráková, M. & Wilson, R. H. (2001). Developments in mid-infrared FT-IR spectroscopy of selected carbohydrates. *Carbohydrate Polymers*, **44**: 291–303.

Katoh, K. & Standley, D.M. (2013). MAFFT Multiple Sequence Alignment Software Version 7: improvements in performance and usability. *Molecular Biology and Evolution*, **30**: 772–780.

Limoges, A., Mertens, K.N., Ruíz-Fernández, A.C. & Vernal, A. (2015). First report of fossilized cysts produced by the benthic *Bysmatrum subsalsum* (Dinophyceae) from a shallow Mexican lagoon in the Gulf of Mexico. *Journal of Phycology*, **51**: 211–215.

Lindberg, K., Moestrup, Ø. & Daugbjerg, N. (2005). Studies on woloszynskioid dinoflagellates I: *Woloszynskia coronata* re-examined using light and electron microscopy and partial LSU rDNA sequences, with description of *Tovellia* gen. nov. and *Jadwigia* gen. nov. (Tovelliaceae fam. nov.). *Phycologia*, **44**: 416–440.

Litaker, W.R., Vandersea, M.W., Kibler, S.R., Reece, K.S., Stokes, N.A., Lutzoni, F.M., Yonish, B.A., West, M.A.,

Black, M.N.D. & Tester, P.A. (2007). Recognizing dino-flagellate species using ITS rDNA sequences. *Journal of Phycology*, **43**: 344–355.

Lombard, E.H. & Capon, B. (1971). *Peridinium gregarium*, a new species of dinoflagellate. *Journal of Phycology*, **7**: 184–187.

Medlin, L., Elwood, H.J., Stickel, S. & Sogin, M.L. (1988). The characterization of enzymatically amplified eukaryotic 16S-like rRNA-coding regions. *Gene*, **71**: 491–499.

Mertens, K.N., Wolny, J., Carbonell-Moore, C., Bogus, K., Ellegaard, M., Limoges, A., de Vernal, A., Gurdebeke, P., Omura, T. & Al-Muftah, A. (2015). Taxonomic re-examination of the toxic armored dinoflagellate *Pyrodinium bahamense* Plate 1906: Can morphology or LSU sequencing separate *P. bahamense* var. *compressum* from var. *bahamense*? *Harmful Algae*, **41**: 1–24.

Moestrup, Ø. & Daugbjerg, N. (2007). On dinoflagellate phylogeny and classification. In *Unravelling the Algae: The Past, Present, and Future of Algal Systematics* (Brodie, J. & Lewis J., editors), 215–230. The Systematics Association Special Volume Series, CRC Press, Boca Raton, FL.

Moestrup, Ø., Hansen, G. & Daugbjerg, N. (2008). Studies on woloszynskioid dinoflagellates III: on the ultrastructure and phylogeny of *Borghiella dodgei* gen. et sp. nov., a cold-water species from Lake Tovel, N. Italy, and on *B. tenuissima* comb. nov. (syn. *Woloszynskia tenuissima*). *Phycologia*, **47**: 54–78.

Mohammad-Noor, N., Daugbjerg, N., Moestrup, Ø. & Anton, A. (2007). Marine epibenthic dinoflagellates from Malaysia – a study of live cultures and preserved samples based on light and scanning electron microscopy. *Nordic Journal of Botany*, **24**: 629–690.

Murray, S., Hoppenrath, M., Larsen, J. & Patterson, D.J. (2006). *Bysmatrum teres* sp. nov., a new sand-dwelling dinoflagellate from north-western Australia. *Phycologia*, **45**: 161–167.

Nézan, E. & Chomérat, N. (2011). *Vulcanodinium rugosum* gen. et sp. nov. (Dinophyceae), un nouveau dinoflagellé marin de la côte méditerranéenne française. *Cryptogamie-Algologie*, **32**: 3–18.

Nézan, E., Tillmann, U., Bilien, G., Boulben, S., Chèze, K., Zentz, F., Salas, R. & Chomérat, N. (2012). Taxonomic revision of the dinoflagellate *Amphidoma caudata*: transfer to the genus *Azadinium* (Dinophyceae) and proposal of two varieties, based on morphological and molecular phylogenetic analyses. *Journal of Phycology*, **48**: 925–939.

Netzel, H. & Dürr, G. (1984). Dinoflagellate cell cortex. In *Dinoflagellates* (Spector, D.L., editor), 43–105. Academic Press, Orlando, FL.

Ostenfeld, C.H. (1908). The phytoplankton of the Aral Sea and its affluents, with an enumeration of the algae observed. *Wissenschaftliche Ergebnisse der Aralsee-Expedition*, **8**: 123–225.

Pandey, K K. (1999). A study of chemical structure of soft and hardwood and wood polymers by FTIR spectroscopy. *Journal of Applied Polymer Science*, **71**: 1969–1975.

Parsons, M.L. & Preskitt, L.B. (2007). A survey of epiphytic dinoflagellates from the coastal waters of the island of Hawai'i. *Harmful Algae*, **6**: 658–669.

Posada, D. (2008). jModelTest: phylogenetic model averaging. *Molecular Biology and Evolution*, **25**: 1253–1256.

Ronquist, F. & Huelsenbeck, J.P. (2003). MrBayes 3: Bayesian phylogenetic inference under mixed models. *Bioinformatics*, **19**: 1572–1574.

Satta, C.T., Anglès, S., Garcés, E., Sechi, N., Pulina, S., Padedda, B.M., Stacca, D. & Lugliè, A. (2013a). Dinoflagellate cyst assemblages in surface sediments from three shallow Mediterranean lagoons (Sardinia, North Western Mediterranean Sea). *Estuaries and Coasts*, **37**: 1–18.

Satta, C. T., Anglès, S., Lugliè, A., Guillén, J., Sechi, N., Camp, J. & Garcés, E. (2013b). Studies on dinoflagellate cyst assemblages in two estuarine Mediterranean bays: a useful tool for the discovery and mapping of harmful algal species. *Harmful Algae*, **24**: 65–79.

Scholin, C.A., Herzog, M., Sogin, M. & Anderson, D.M. (1994). Identification of group- and strain-specific genetic markers for globally distributed *Alexandrium* (Dinophyceae). II. Sequence analysis of a fragment of the LSU rRNA gene. *Journal of Phycology*, **30**: 999–1011.

Selwood, A.I., Wilkins, A.L., Munday, R., Gu, H., Smith, K.F., Rhodes, L.L. & Rise, F. (2014). Pinnatoxin H: a new pinnatoxin analogue from a South China Sea *Vulcanodinium rugosum* isolate. *Tetrahedron Letters*, **55**: 5508–5510.

Spurr, A.R. (1969). A low-viscosity epoxy resin embedding medium for electron microscopy. *Journal of Ultrastructure Research*, **26**: 31–43.

Stamatakis, A. (2006). RAxML-VI-HPC: maximum likelihood-based phylogenetic analyses with thousands of taxa and mixed models. *Bioinformatics*, **22**: 2688–2690.

Steidinger, K. A. & Balech, E. (1977). *Scrippsiella subsalsa* (Ostenfeld) comb nov. (Dinophyceae) with a discussion on *Scrippsiella*. *Phycologia*, **16**: 69–73.

Swofford, D.L. (2002). PAUP*. Phylogenetic analysis using parsimony (* and other methods), version 4. Sinauer Associates, Sunderland, MA.

Ten-Hage, L., Quod, J., Turquet, J. & Couté, A. (2001). *Bysmatrum granulosum* sp. nov. a new benthic dinoflagellate from the southwestern India sea. *European Journal of Phycology*, **36**: 129–135.

Tillmann, U., Elbrächter, M., Krock, B., John, U. & Cembella, A. (2009). *Azadinium spinosum* gen. et sp. nov. (Dinophyceae) identified as a primary producer of azaspiracid toxins. *European Journal of Phycology*, **44**: 63–79.